In situ AFM study of the interaction between calcite $\{10\bar{1}4\}$ surfaces and supersaturated Mn^{2+}–CO_3^{2-} aqueous solutions

Carlos Pérez-Garrido [a], José Manuel Astilleros [a,*], Lurdes Fernández-Díaz [a], Manuel Prieto [b]

[a] Departamento de Cristalografía y Mineralogía, Universidad Complutense de Madrid, 28040 Madrid, Spain
[b] Departamento de Geología, Universidad de Oviedo, 33005 Oviedo, Spain

ABSTRACT

Growth of rhodochrosite ($MnCO_3$) on calcite $(10\bar{1}4)$ substrates from supersaturated aqueous solutions was observed in situ using an atomic force microscope (AFM). The supersaturation with respect to rhodochrosite (expressed as $\beta_{rhod} = a[Mn^{2+}]a[CO_3^{2-}]/K_{sp,\ rhod.}$; where $a[Mn^{2+}]$ and $a[CO_3^{2-}]$ are the activities of Mn^{2+} and CO_3^{2-} in the aqueous solution) ranged from 48.89 to 338.04. After an induction period, nuclei of the new phase are formed on the calcite substrate. These nuclei readily reach a significant height (2.2 + 0.2 nm), which remained approximately constant during their lateral spread. The characteristics of the growth pattern of islands of the newly formed phase indicate that there exists an epitaxial relationship between the new phase and the calcite substrate. The islands show a highly anisotropic growth, preferentially spreading along $[42\bar{1}]$ on the calcite substrate at a rate up to 15 times faster than along [010]. As a result, the islands develop needle and sword blade-like morphologies, elongated along $[42\bar{1}]$ and showing different truncated ends. This unusual elongation is interpreted as the result from a kinetic effect, which is controlled by both the structural characteristic of the calcite $(10\bar{1}4)$ surface and the structure and elastic properties of the overgrowing phase. The lateral growth of islands leads to their coalescence and the formation of a quite homogeneous nanometric layer. The characteristics of the epitaxial growth are in agreement with a Volmer–Weber growth mechanism controlling the formation of the epitaxy. The results obtained in these experiments are compared with those obtained in several similar systems.

Keywords:
A1. Atomic force microscopy
A1. Supersaturated solutions
A2. Growth from solutions
B1. Calcite
B1. Rhodochrosite
A3. Volmer–Weber growth mechanism

1. Introduction

A special extensive phenomenon observed both in nature and laboratory is the formation of solid solutions grown from multicomponent aqueous solutions, which often results in the formation of crystals with complicated compositional zoning patterns [1–3]. Such patterns frequently consist of a sharp alternation of layers with very similar crystal structure, but with substantial differences in chemical composition and lattice constants. In the last analysis, the formation of zoning patterns is determined by the aqueous solution–crystal interface interactions occurring during the growth. Although much research has been dealt with the study of such interaction, the ultimate molecular factors involved in the development of compositional patterns are still not completely understood. The nanotopographic features of a growing phase are the result of changes in both the predominant growth mechanism and the growth rate due to different factors. The incorporation of growth units with different compositions is among the factors that have a stronger effect. Regarding this, various works [4,5] have reported nanoscale observations, which indicate that the substrate also exerts a strong effect on the growth rate of layers forming from a multicomponent aqueous solution. The control exerted by the substrate is referred to as "template effect" [5,6]. It involves the retard of the step growth rate of successive monolayers that spread on a pure substrate. The progressive retardation of the step velocity can lead to the stoppage of growth after a few new layers have been completed. The recovering of growth after its complete stoppage can be related to an increase in the supersaturation and may involve a sharp change in the composition of the new layer. A sequence of similar events may be the basis of the development of zoning patterns, especially in the case of those that show high compositional gradients between adjacent zones. In other words, the development of oscillatory zoning patterns might be a consequence of successive events of heteroepitaxial growth, each one initiated after a complete stoppage of the growth due to the factors controlled by the substrate.

This paper represents a new contribution to the study of the development of epitaxial relationships during growth in solid

* Corresponding author. Tel.: +34 91 3944881; fax: +34 91 3944872.
E-mail addresses: carlospgarrido@geo.ucm.es (C. Pérez-Garrido), jmastill@geo.ucm.es (J.M. Astilleros), lfdiaz@geo.ucm.es (L. Fernández-Díaz), mprieto@geol.uniovi.es (M. Prieto).

solution–aqueous solution (SS–AS) systems [7,8], focusing on the processes occurring when one end-member of the solid solution directly grows on a substrate with the characteristics of the opposite end-member. Here, we use an approach that we have previously applied to other SS–AS systems [9,10]. In this case, the Mn–Ca–CO_3–H_2O system is addressed. The two carbonate phases involved, rhodochrosite ($MnCO_3$) and calcite (the stable $CaCO_3$ phase at 25° and 1 atm.), are isomorphic, with the following lattice constants: a_{hex}=4.988 Å, c_{hex}=17.068 Å for calcite and a_{hex}=4.772 Å, c_{hex}=15.637 Å for rhodochrosite [11]. These compounds form a solid solution crystallizing in the trigonal space group $R\bar{3}c$. In this system, also the double salt kutnahorite ($MnCa(CO_3)_2$), with a dolomite-type structure, exists. Although this system has been thoroughly studied [6,12,13], many uncertainties with respect to both the extent and non-ideality of the solid solution and the stability field for kutnahorite still remain. Furthermore, an agreement with respect to the solubility product of the end-member rhodochrosite still has to be reached, with a number of values, ranging from $K_{sp,\ rhod}=10^{-9.43}$ [13] to $K_{sp,\ rhod}=10^{-12.51}$ [14], having been proposed.

Several previous works have approached the study of interaction processes of Mn-bearing aqueous solution with calcite surfaces at the nanoscale. Astilleros et al. [6] studied the direct growth of a (Mn, Ca)CO_3 solid solution on the calcite cleavage substrate using Mn-bearing solutions supersaturated with respect to calcite. Jun et al. [15] studied the precipitation of manganese oxides on the calcite ($10\bar{1}4$) surface by adding a stock Mn^{2+} (aq) solution previously purged with oxygen. In addition, Lea et al. [16] investigated the interaction of low concentrated Mn-bearing solutions undersaturated with respect to calcite with a calcite ($10\bar{1}4$) substrate. They observed the simultaneous nucleation and subsequent epitaxial formation of multilayer three-dimensional islands, which they interpreted as corresponding to kutnahorite.

In this work, we aim to investigate the epitaxial growth of rhodochrosite on a calcite ($10\bar{1}4$) substrate at the molecular scale. With this intention, we have carried out series of AFM experiments putting aqueous solutions supersaturated with respect to $MnCO_3$ in contact with the calcite substrate. The changes in the nanotopographic features have been monitored by collecting AFM images at defined intervals. The growth process has been observed considering a wide range of supersaturations with respect to rhodochrosite. The crystallography relationships between the new phase and the substrate, as well as the characteristics of the newly formed nuclei (height and shape) have been established. Finally, direct measurements of island growth rates allow us to draw a complete picture of the growth process.

2. Experimental

Natural optically clear calcite crystals (Iceland spar quality) were cleaved on ($10\bar{1}4$) and placed inside the fluid cell of an AFM (Digital Instruments, Nanoscope IIIa, Multimode). Before each growth experiment, deionised water (18.2 MΩ · cm, Milli-Q) was passed over the crystal to clean the cleaved ($10\bar{1}4$) calcite surface, as well as to adjust the AFM parameters. Growth solutions were prepared immediately prior to the start of each experiment by mixing Na_2CO_3 and $MnCl_2$ (Panreac, reactive grade) solutions. In order to avoid changes in the manganese oxidation state, Mn reaction solutions were saturated with N_2 at room temperature by bubbling with nitrogen gas for at least 1 h. The pH value of the supersaturated solutions was determined using a Eutech Instruments pH meter (model pH 6) with a pH meter electrode calibrated with 7.00 and 10.00 buffers (Crison). The fluid cell was filled with a supersaturated aqueous solution containing

Table 1
Initial concentrations of $MnCl_2$, Na_2CO_3 and activities in μmol/l, pH and supersaturation ($\beta_{rhod.}$).

Experiment	$[MnCl_2]$	$[Na_2CO_3]$	$a[Mn^{2+}]$	$a[CO_3^{2-}]$	$pH_{solution}$	β_{rhod}
M05C1a	50	100	1.39	1.31	10.1	48.89
M1C1a–e	100	100	4.33	0.71	10.1	83.18
M1C2a–e	100	200	1.47	3.15	10.1	120.23
M1C3a–f	100	300	0.66	7.42	10.2	138.04
M13C3a	130	300	1.08	6.05	10.2	173.78
M2C1a–b	200	100	12.18	0.36	10.2	120.23
M2C2a–e	200	200	6.88	1.28	10.1	204.17
M2C3a–f	200	300	3.18	3.44	10.2	257.04
M3C1a–b	300	100	20.30	0.25	10.1	138.04
M3C3a–h	300	300	9.13	1.75	10.2	338.04

Mn^{2+} and CO_3^{2-}, which was maintained static in the cell with no flow through the system. The volume of the fluid cell is 50 μL. Measurements on sequences of AFM images recorded at intervals of 50–60 s allow us to quantify the nanotopographic changes occurring during the growth process. Both the initial compositions of the aqueous solutions and the supersaturation with respect to rhodochrosite (expressed as $\beta_{rhod}=a[Mn^{2+}]a[CO_3^{2-}]/K_{sp,\ rhod.}$; where $a[Mn^{2+}]$ and $a[CO_3^{2-}]$ are the activities of Mn^{2+} and CO_3^{2-} in the aqueous solution) are shown in Table 1. The rhodochrosite solubility product used was that provided in the PHREEQC database ($K_{sp,\ rhod.}=10^{-11.13}$), included in the PHREEQC-2 speciation solubility geochemical code [17]. All experiments were conducted at room temperature and most of them lasted longer than 1 h. All the AFM images shown in this work were taken in constant force mode while displaying both cantilever height and deflection signals. The scanned area ranged from 5 × 5 to 15 × 15 μm. The scan time for each image was approximately 1 min with a scan rate of 5.2 Hz. Silicon nitride tips (Veeco NP-S10) with a nominal force constant k=0.06–0.58 N/m were used.

3. Results

The direct observation of the development of the etch pits forming on calcite ($10\bar{1}4$) surface in contact with pure water allows us to establish the main crystallographic directions on the calcite substrate. According to numerous studies, the shape of these etch pits is defined by edges that run parallel to the most stable "Periodic Bond Chains" (PBCs) [18–24]. The retreat of the edges of these etch pits is highly anisotropic, with a pair of steps retreating rapidly and the other one retreating very slowly. The anisotropy of the retreat of the edges during dissolution is a consequence of the inequivalence of the two pairs (positive and negative) of opposing straight steps parallel to the [$\bar{4}41$] and [$48\bar{1}$] directions (see Fig. 1) [24–26]. Thus, while the "negative" [$\bar{4}41$]$_-$ and [$48\bar{1}$]$_-$ steps overhang the underlying layer defining an acute angle (78°) that contains constrained kink sites, the "positive" [$\bar{4}41$]$_+$ and [$48\bar{1}$]$_+$ steps define an obtuse angle (102°) that contains open kink sites. The obtuse (positive) steps are more reactive [27] and their retreat velocity is much faster than that of the acute (negative) steps.

Despite the fact that all the growth solutions used in this work are undersaturated with respect to calcite, no dissolution of the calcite substrate is observed after injecting any of them in the fluid cell, irrespective of the interaction period considered. Thus, both the cleavage steps and the etch pits edges remain virtually static during the whole interaction process between the ($10\bar{1}4$) calcite surface and the growth solution (see growth sequences in Figs. 3 and 7).

The initial stages of the interaction process between the growth solution and the ($10\bar{1}4$) calcite surface differ depending

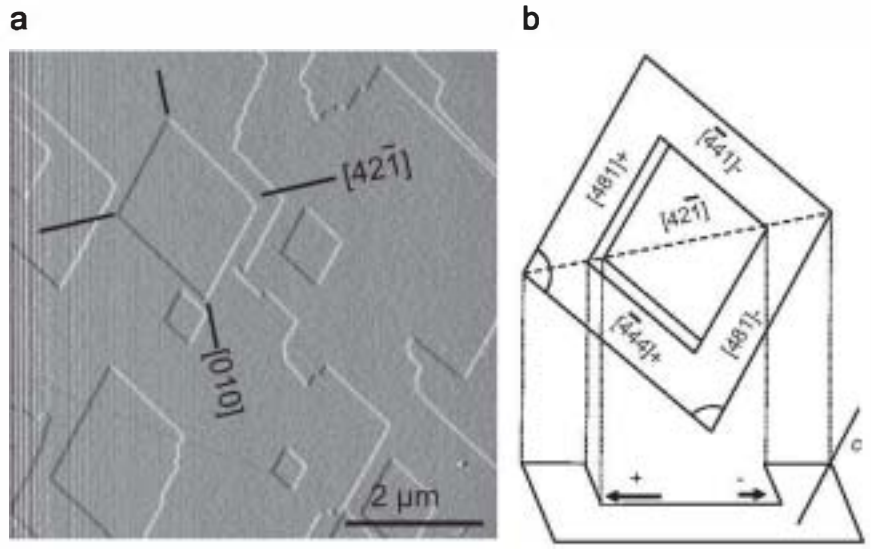

Fig. 1. AFM deflection image of a calcite (10$\bar{1}$4) surface dissolving in pure water. On the dissolution pit, four non-equivalent steps parallel to the $\langle\bar{4}41\rangle$ directions define a rhombus shape. The two adjacent steps ([48$\bar{1}$] and [$\bar{4}$41]) overhang the underlying layer defining an acute angle, while the other two adjacent steps ([48$\bar{1}$]$_+$ and [$\bar{4}$41]$_+$) define an obtuse angle. The long and the short diagonals of the rhombus run parallel to [010] and [42$\bar{1}$] directions, respectively.

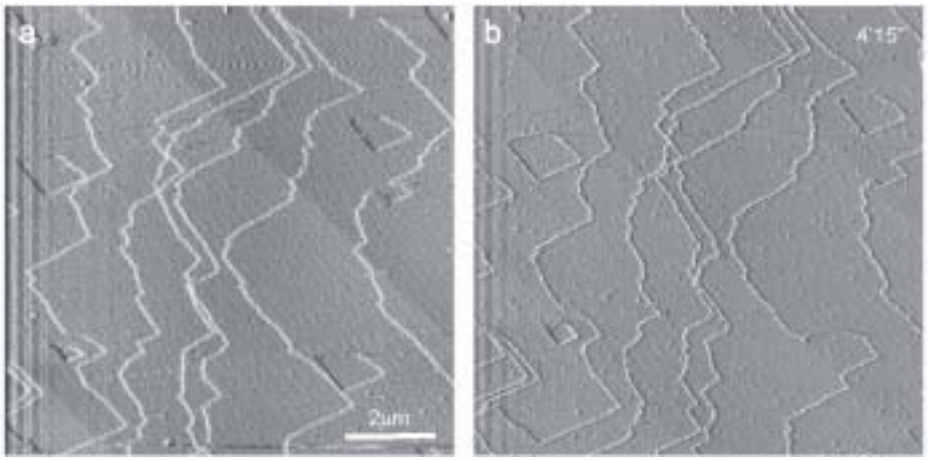

Fig. 2. (a) AFM deflection image of calcite (10$\bar{1}$4) surface (a) after dissolving with deionised water and (b) after ~5 min of interaction with the growth solution (Exp. M2C2a, static solution), small nuclei are formed on the calcite surface, mainly decorating the cleavage and pit steps, but also on the terrace.

on the initial concentration of Mn. Thus, when such concentration is high ($\beta_{rhod} > 100$), the formation of a precipitate is immediately observed. This precipitate consists of nuclei with undefined shapes and variable heights, ranging from 0.22 to 0.94 nm. The nuclei mainly decorate the cleavage steps and the edges of the etch pits in the calcite substrate. However, some nuclei can also be observed homogeneously distributed on the terraces (Fig. 2). Their adhesion to the substrate is low, which explains that they are partially removed by the AFM-tip during the scanning. Few minutes after their formation, these nuclei start to dissolve and readily disappear. From this point the behaviour observed coincides in all the experiments, whatever the initial Mn concentration in the aqueous solution is. Then new nuclei corresponding to a different phase are formed on the calcite substrate. As can be seen in Fig. 3, where a representative sequence of both the formation and the subsequent growth of these nuclei is shown, the nuclei appear homogeneously distributed on the substrate. The growth of the nuclei rapidly leads to the development of islands, bounded by well-defined edges and showing a characteristic elongated morphology. These islands reach a significant height (2.2 ± 0.2 nm) in the first minutes after their formation, thus becoming three-dimensional. During their lateral spread, these islands maintain an approximately constant height. Therefore, we will refer to them hereafter as three-dimensional (3D) islands, following the term used by Chernov [28] to describe multilayer islands in epitaxial growth processes. Fig. 4 shows a striking example of the homogeneity of the islands' height. In the AFM height image, eight different 3D-islands can be observed, with their height varying between 2.16 and 2.35 nm.

The orientation of the growing islands with respect to the substrate indicates the existence of a clear crystallographic relationship between the new phase and the calcite (10$\bar{1}$4) surface. Such a relationship can be clearly identified by observing the images shown in Fig. 5, where the crystallographic directions along the etch pit steps are indicated. The 3D-islands preferentially grow parallel to [42$\bar{1}$], while they show a very limited development along the perpendicular direction, [010] on the calcite substrate. Such an anisotropic growth rapidly leads to

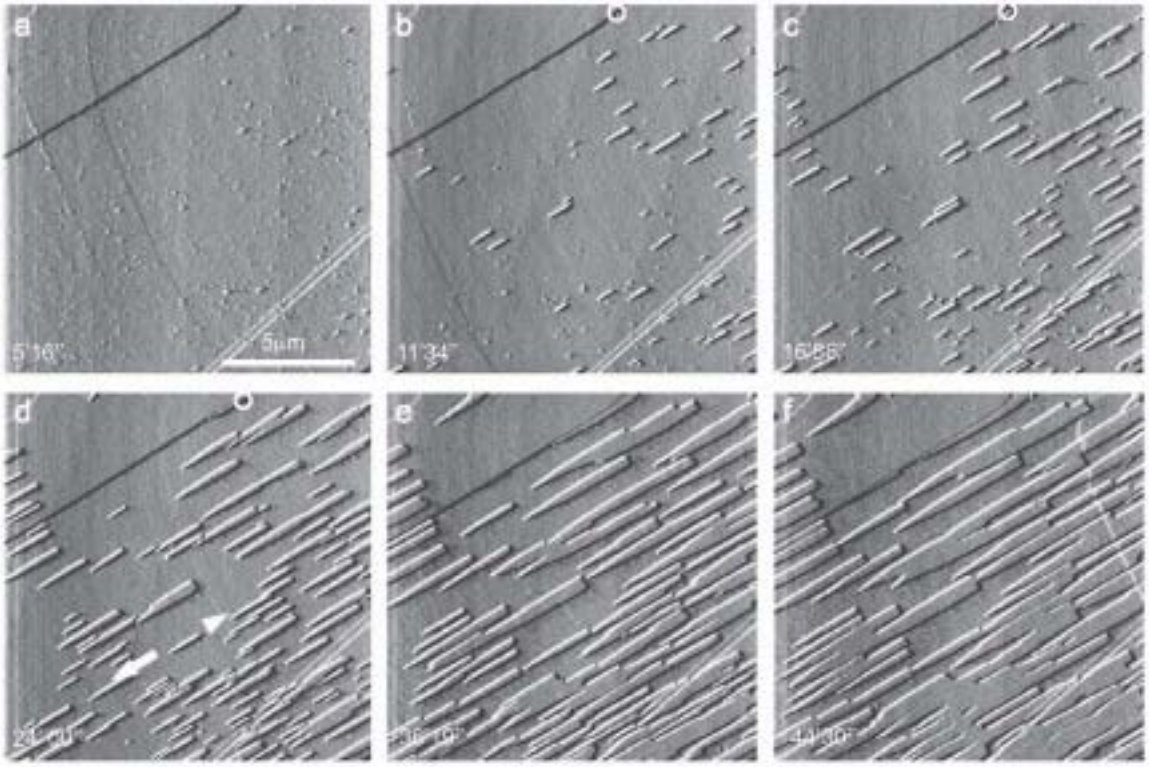

Fig. 3. AFM deflection sequence showing the nucleation and subsequent growth of 3D-islands on a calcite $(10\bar{1}4)$ face from Exp. M1C3a (see Table 1). (a–c) The formation and growth of nuclei leads to the development of elongated needle-shaped islands, which grow preferentially parallel to $[42\bar{1}]$. (d–e) The growth along this direction is anisotropic (see white arrows) and islands exhibit a sword blade-like shape. (f) The lateral spread of the islands leads to their coalescence and the formation of a quite homogeneous nanometric layer. Elapsed times from the injection of growth solution are shown in the bottom left-hand corner of each AFM image.

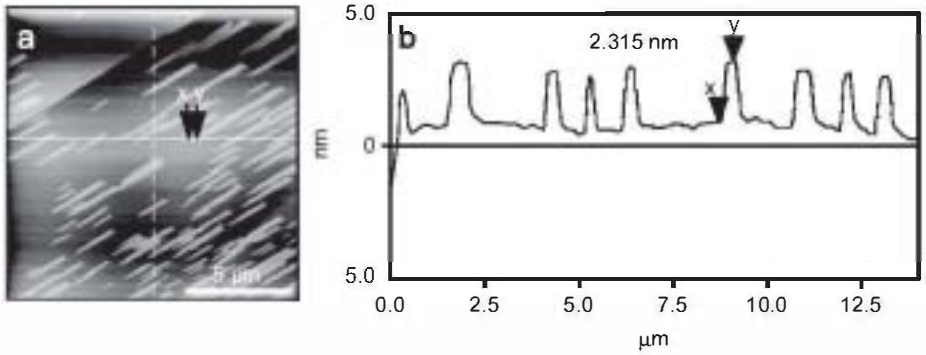

Fig. 4. (a) AFM height image showing the formation of thick islands on calcite $(10\bar{1}4)$ surface (Exp. M1C3a). (b) Height profile along the solid line in (a). The vertical distance between the triangular pointers "*x*" and "*y*" indicates the height of a three-dimensional island, ~2.3 nm.

the development of elongated needle-like shapes, which can be clearly observed in Fig. 3. By comparing the change in island sizes with the edges of the etch pits previously formed on the calcite substrate, which can be used as a reference since no dissolution is observed at this stage, it can be concluded that the 3D-islands spread faster from their (+/+) corners (see caption of Fig. 8 for explanation). The anisotropic growth within the $[42\bar{1}]$ direction determines that the needle-like islands become differently truncated at their ends. Thus, whereas the fast end becomes sharp and develops a thin tip, the opposite one appears blunt and thicker. As a result, the 3D-islands rapidly achieve a sword blade-like shape (Figs. 3b–f).

The lateral spread of the islands dominates their growth, since the formation of 2D-nuclei on top of these islands is very limited. The lateral spread of the 3D-islands leads to their coalescence, which is commonly complete after around one hour after the formation of the first nuclei. Such coalescence causes the formation of a homogeneous nanometrically flat layer of the newly formed phase. This layer finally completely armours the calcite substrate from interaction with the solution (Fig. 6). At this point, the advancement of the scarce monolayers (with a height similar to the covered calcite steps) formed on top of the 3D-islands is strongly retarded, the step edges become scalloped and the growth process virtually stops few minutes after the completion of the substrate-covering layer. In order to dismiss that the retardation of the monolayers' advancement could be caused by a significant decrease in the supersaturation of the aqueous solution for rhodochrosite, fresh solutions were injected

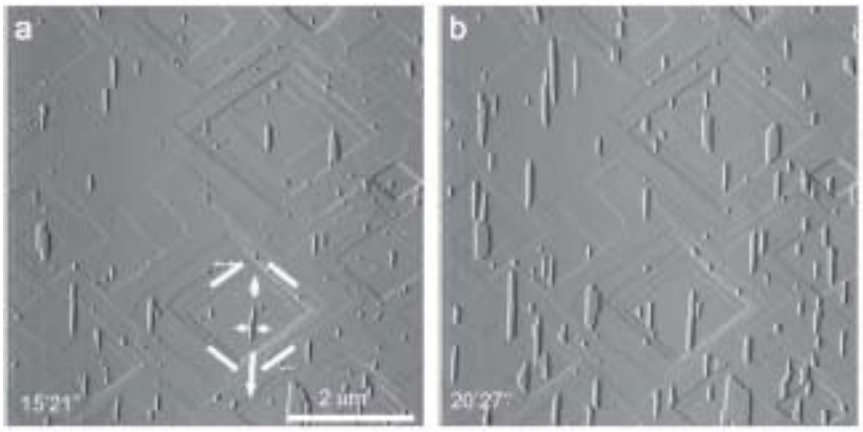

Fig. 5. (a–b) Sequence of AFM deflection images showing the spread of 3D-islands on calcite $(10\bar{1}4)$ surface (Exp. M3C3a). Orientation of the islands and sense of anisotropic growth along $[42\bar{1}]$ can easily be established using pits as a reference. Elapsed times from the injection of the growth solution are shown in the bottom left-hand corner of each AFM image.

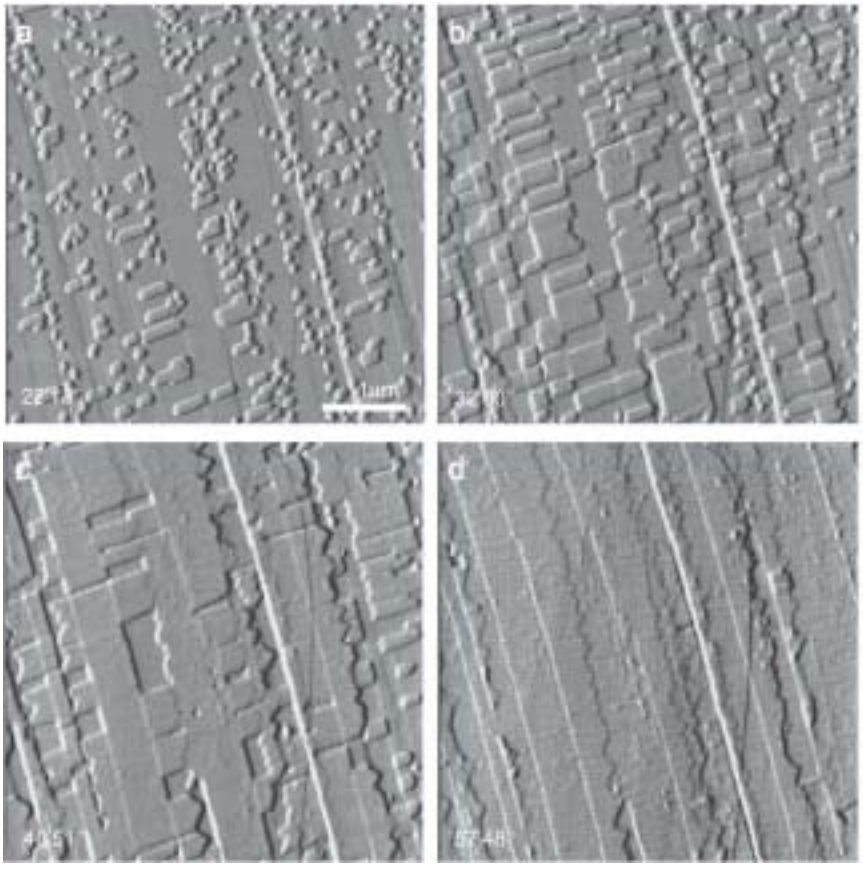

Fig. 6. (a–c) AFM deflection images showing 3D-islands growing on a calcite (Exp. M3C3f). The islands grow elongated along $[42\bar{1}]$ direction. Islands always remain uniform in height during their lateral spread and after coalescence they reproduce nanotopographic features (cleavage steps) of the underlying calcite surface. (d) The step edges of monolayers advancing on top of the 3D-islands become scalloped and the growth process virtually stops few minutes later. Elapsed times from the injection of the growth solution are shown in the bottom left-hand corner of each AFM image.

in the fluid cell after the completion of the 3D-islands coalescence. In no experiment either the formation of new islands or the increase in the spread rate of the pre-existing monolayers were detected.

The layer of the newly formed phase perfectly reproduces every detail of the original nanotopography in the calcite substrate. This can be clearly observed in images shown in Fig. 7, where after the coalescence of 3D-islands the underlying cleavage steps and the etch pits edges, corresponding to the calcite substrate, are still identifiable after the formation of the nanometric layer.

4. Discussion

The interaction between $(10\bar{1}4)$ calcite surfaces and aqueous solutions supersaturated with respect to rhodochrosite leads to the development of a number of surface processes, which occur

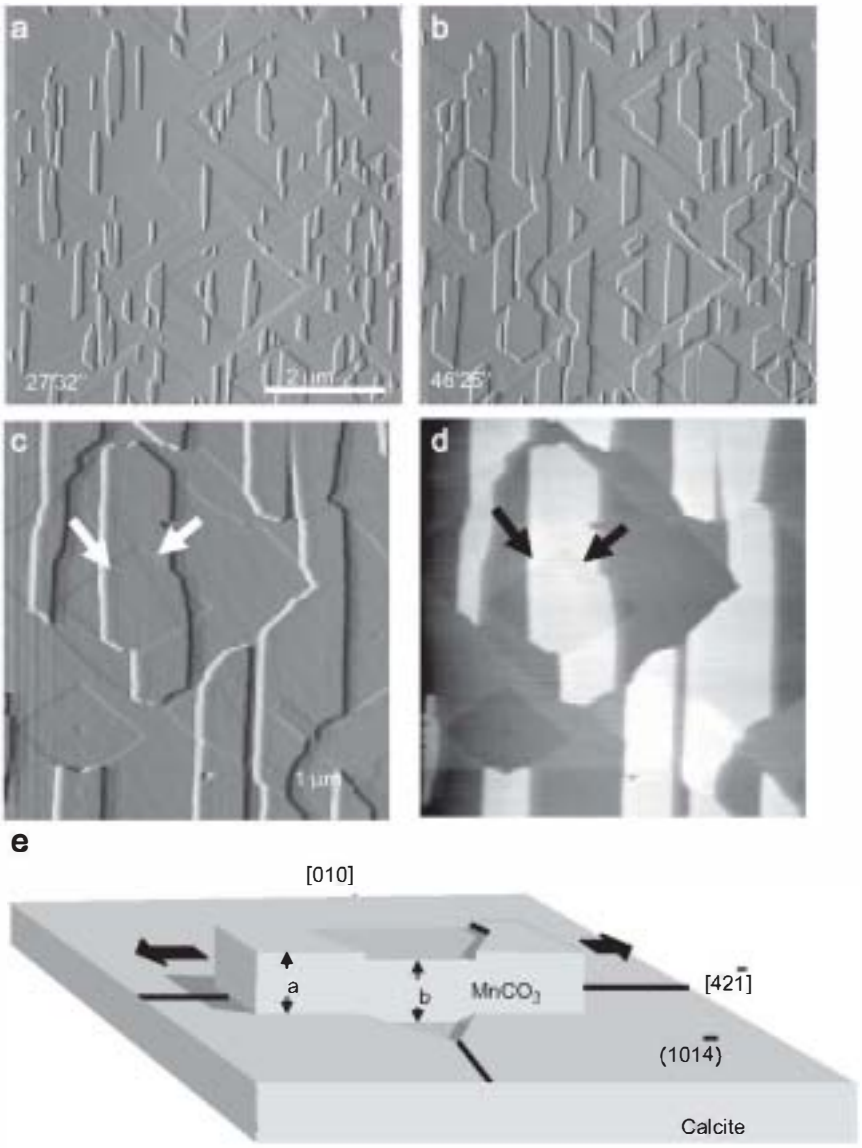

Fig. 7. (a–b) Sequence of AFM deflection images showing the spreading of 3D-islands on a calcite $(10\bar{1}4)$ surface (Exp. M3C3a). The coalescence of islands leads to the formation of a homogeneous layer that appears as large patches on the surface. (c) Detail of 3D-islands growing on a calcite surface after 45 min of interaction. The islands grow elongated along $[42\bar{1}]$ direction. Islands always remain uniform in height during their lateral spread and after coalescence they reproduce nanotopographic features (cleavage and etch pits steps) of the underlying calcite surface (see arrows). (d) Height AFM image corresponding to the same area. (e) Sketch illustrating the crystallographic orientation of a three-dimensional nucleus produced after the coalescence of several nuclei on calcite $(10\bar{1}4)$ surface. The coalescence of nuclei formed on differenttopographic heights (pits and terraces) leads to the exact reproduction of the underlying topography (but 2.2 nanometers above). This phenomenon can only take place if the height of the nuclei are the same (see distances "*a*" and "*b*") and remains uniform during the growth process. The lateral scales on each surface are greatly underestimated relative to the scale normal to the surface. However, the height of the pit and the growing layer are done to scale with respect to each other.

sequentially and, in some cases, can overlap. Among these processes the most significant ones are (1) inhibition of calcite dissolution, (2) under initial high Mn concentrations, initial formation of a precipitate that disappear after a short interaction time and (3) the formation of elongated 3D-islands of constant thickness.

4.1. Inhibition of calcite dissolution

As mentioned above, no dissolution has been observed in any of the experiments carried out when the calcite substrate is in contact with a growth solution, despite the fact that all the aqueous solutions used were undersaturated with respect to calcite. Our observations are in agreement with the results obtained by different authors on the influence of metal cations on the kinetics of calcite dissolution. Macroscopic studies [29,30] have shown that the calcite dissolution rate is highly dependent on the concentration of cationic impurities, with the metal divalent cations smaller than Ca^{2+}, i.e. those which form carbonates with calcite-type structure, being the most efficient as inhibitors of calcite dissolution. Moreover, AFM observations carried out by Lea et al. [31] and Vinson et al. [32] indicate that the presence of small amounts of Mn^{2+} in an aqueous solution can drastically reduce the step-edge migration rates and, if a sufficient amount of CO_3^{2-} is available in the solution, can lead to the virtual stoppage of the calcite dissolution. Such a strong effect is interpreted due to the adsorption of ions onto the surface, followed by a rapid diffusion to specific sites, which are then blocked by them. Moreover, the enhancement of the Mn effect as

calcite dissolution inhibitor by the presence of CO_3^{2-} anions is interpreted as the result from a strong affinity between Mn^{2+} and CO_3^{2-}. Whereas in the solution such an affinity leads to the formation of a strong complexing ligand ($MnCO_3^0$), on the $(10\bar{1}4)$ calcite surface it may control the formation of a similar surface complex, which would stabilize the reactive sites. This interpretation is also supported by the results obtained in the present work.

4.2. Nature and composition of the precipitates

The processes observed when the growth solution is in contact with the calcite substrate depend on the initial supersaturation with respect to rhodochrosite. As mentioned above, when this supersaturation is high ($\Omega_{rhod} > 100$), the formation of a precipitate rapidly occurs. However, this precipitate disappears after a short period, probably as a result of the combination of dissolution and removal by the tip. Immediately, 3D-islands of a different phase grow. When the initial supersaturation with respect to rhodochrosite is lower than 100, no initial formation of a precipitate is observed and 3D-islands are formed directly. The nature of both the initial precipitate and the 3D-islands needs to be discussed separately. In order to achieve general conclusions, we combine different approaches. It is important to note that, although in the particular case of metal–calcite interactions there is a vast amount of information in the scientific literature, comprising scales and techniques in the range from the macro- to the nanoscopic scale, very frequently the application of high resolution surface analysis techniques like X-ray photoelectron spectroscopy (XPS), electron paramagnetic resonance or energy dispersive X-ray spectroscopy in the determination of the actual chemical composition of the precipitates grown on a mineral surface is not yet conclusive [16]. Moreover, indirect information based on the evolution of the nanotopographic features can be in some cases more significant to achieve conclusions on the nature of the newly formed phases.

4.2.1. Nature of the small nuclei formed at high Mn concentrations

The nature of these small nuclei is especially difficult to elucidate. It may be hypothesized that they correspond to rhodochrosite, epitaxially grown on the calcite cleavage surface to form a "wetting layer", according to the Stransky–Krastanov mechanism for epitaxies. However, the fact that the nuclei do not inherit any of the growth characteristics of the calcite surface, together with the large variability of the height values measured on these nuclei (0.22–0.94 nanometers), do not support this hypothesis.

Another possibility is that the nuclei correspond to oxides, which would form as a consequence of the brief contact of the growing solution with the atmosphere at the moment of its injection into the fluid cell. A third possibility is that the nuclei correspond to Mn-hydroxides. Although the nature of these nuclei cannot be categorically stated on the basis of our observations, this last hypothesis seems to be the most plausible. The low PO_2 in the solution after bubbling N_2 should prevent the formation of oxides. However, the formation of Mn-hydroxides can be explained as a consequence of the precipitation occurring under high pH conditions, which would be locally achieved as a result of the rapid reaction of the aqueous solution with the calcite surface. It is important to note that the supersaturation of the solution with respect to $Mn(OH)_2$ rapidly increases with pH. In addition, the oxygen–oxygen and metal–oxygen bond lengths on calcite structure are much more similar to those in the manganese hydroxide than to the bond lengths in the Mn-oxides [15]. Consequently, the lower mismatch between Mn-hydroxide nuclei and the calcite cleavage surface would also point at these nuclei being interpreted as Mn-hydroxide.

4.2.2. Nature and composition of the oriented 3D-islands

The 3D-islands show the typical rhombohedral morphology and the anisotropic growth, which correspond to that observed in different rhombohedral carbonate phases [8,33], inheriting characteristics of the growth behaviour of the calcite surface. In addition, the height of the monolayers formed on top of the 3D-islands, as described in Fig. 6, is similar to that of calcite monolayers. The fact that dissolution of the calcite surface has never been observed in our experiments after the injection of the growth solution, irrespective of the length of the interaction period considered (see growth sequences in Figs. 3 and 7 and previous discussion), points at virtually no ions being released to the aqueous solution from the calcite substrate. This means that the composition of the growth solution is not significantly chemically affected by the substrate crystal during the growth process of the 3D-islands. Since no calcium is being released on the growth solution, any phase whose composition contains a significant amount of calcium (either kutnahorite or any Ca-rich member of the $(Mn,Ca)CO_3$ solid solution) cannot be possibly form. Therefore, it can be concluded that the nature of the 3D-islands coincides with that of the phase for which the solution is supersaturated, i.e. rhodochrosite.

4.3. Morphology, thickness and epitaxial growth mechanism of the islands

Rhodochrosite islands show a clear epitaxial relationship with the calcite substrate, with the islands growing strongly elongated along $[42\bar{1}]$ and showing no edges parallel to $[\bar{4}41]$ and $[48\bar{1}]$. The epitaxial relationship is favoured by the fact that both phases are isostructural. However, the morphology of the islands is peculiar. As has been pointed out by a number of authors [26,34], the PBCs running along $[\bar{4}41]$ and $[48\bar{1}]$ are straight and steps parallel to these directions contain a low density of kinks. On the contrary, along $[42\bar{1}]$ and [010] PBCs are rougher, with a much higher density of kinks. The lower the kink density, the lower is the growth rate and, finally, the higher the relative probability of development of the corresponding edges [35], one should expect rhodochrosite 3D-islands to show a typical rhombus-shape, bounded by edges parallel to $[\bar{4}41]$ and $[48\bar{1}]$. The apparent contradiction between the morphology expected and that shown by the rhodochrosite 3D-islands cannot be easily explained on the basis of either the linear lattice misfits between the overgrowth and the substrate along different directions nor by the normal kinetics of different steps on $(10\bar{1}4)$ surface. Thus, in the case of rhodochrosite structure, the distance between neighbouring CO_3^{2-} ions is 3.798 Å along the $[42\bar{1}]$ directions, 4.777 Å along [010] and 6.102 Å along $[\bar{4}41]$ and $[48\bar{1}]$ (see Fig. 8). The comparison of these values to those of calcite structure indicates that the smallest mismatch between both structures within the contact plane $(10\bar{1}4)$ exists along [010] (4.33%), the direction along which the 3D-islands show the slowest growth rate. On the contrary, the highest lattice mismatch, 9.78%, exists along $[42\bar{1}]$, the direction of elongation of the islands and, consequently, along which preferential growth occurs. For the other PBC directions, $[\bar{4}41]$ and $[48\bar{1}]$, the calculated linear lattice mismatch is 5.28%, with an additional small angular mismatch because of $\sim 1.0°$ difference in the angle between $[\bar{4}41]$ and $[48\bar{1}]$ in both structures.

The peculiar characteristics of the epitaxially grown rhodochrosite islands coincide with the main features of the kutnahorite [16] and otavite [8] islands grown on calcite $(10\bar{1}4)$ surfaces.

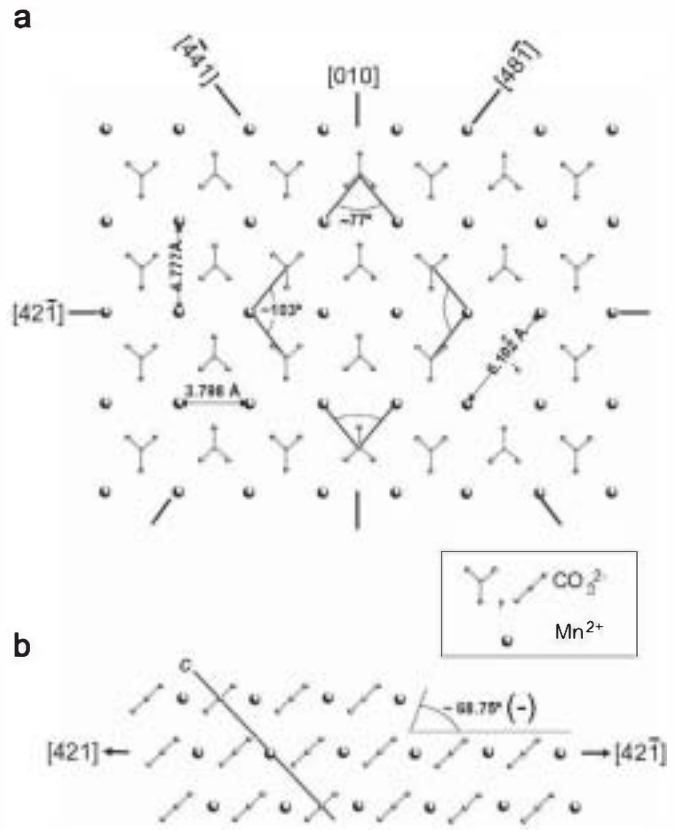

Fig. 8. (a) Schematic of the (10$\bar{1}$4) surface of rhodochrosite with dimensions angles and PBC directions indicated. The [42$\bar{1}$] direction runs parallel to the short diagonal of the rhombus defined by to $\langle\bar{4}41\rangle$ and $\langle48\bar{1}\rangle$ directions. The [010] direction parallels the long diagonal. The rhodrochrosite islands show a marked elongation along [42$\bar{1}$]. (b) Projection of the calcite structure perpendicular to [010] and along [42$\bar{1}$] showing the acute angle (−). Islands migrate faster along the less constrained sites (+/+).

In order to solve the apparent contradiction between the observed shape of the rhodochrosite islands and both the characteristics of the rhodochrosite–calcite lattice mismatch and the typical step growth kinetics within (10$\bar{1}$4) surfaces in calcite-type structures, it is necessary to take into account (i) the elastic properties of the rhodochrosite structure and (ii) a possible kinetic effect, related to the preferential adsorption of Mn^{2+} in specific sites on calcite (10$\bar{1}$4). In relation to the elastic properties of calcite and dolomite-type structures, Lea et al. [16] considered the preferential elongation along [42$\bar{1}$] of pseudokutnahorite islands as a consequence of the smaller stiffness of this direction (around a 30% lower than along the [010] direction), which may partially compensate the higher mismatch between overgrowth and substrate [36]. The elastic "weakness" of [42$\bar{1}$] direction may also favour the faster spread of rhodochrosite islands along this direction on the calcite substrate. Another factor favouring the elongating of rhodochrosite islands along [42$\bar{1}$] possibly relates to the preferential inhibition of growth at the (±) corners where obtuse and acute steps join, i.e. where regions with different types of kinks contact each other. Such inhibition will contribute to stabilize steps parallel to [42$\bar{1}$]. A similar interpretation has been given by a number of authors [31,33,37–39] to the morphological evolution of etch pits, during dissolution, and to the stabilization of certain edges, during growth, on (10$\bar{1}$4) calcite surface in contact with aqueous solutions containing divalent cations smaller than Ca^{2+}. Moreover, the different reactivities of different types of sites can also account for the anisotropic growth within [42$\bar{1}$]. On this direction, two types of kink sites can be distinguished: open (+/+) kinks, located where obtuse steps ([$\bar{4}41$]$_+$ and [48$\bar{1}$]$_+$) join and the constrained (−/−) kinks, where acute steps ([$\bar{4}41$]$_-$ and [48$\bar{1}$]$_-$) join (see Figs. 1 and 8b). Open (+/+) sites are more reactive than (−/−) sites. As a result, growth units will preferentially incorporate into (+/+) sites. Such a preferential incorporation will result in a faster spreading of the tip of the islands where (+/+) sites are located. As a consequence, rhodochrosite islands will develop the sword blade-like shape. This is evidenced in Fig. 5, using as a reference both the steps of etch pits on the calcite substrate and the islands growing inside the pits.

The islands become three-dimensional during the very initial stages of their growth, reaching a thickness of about 8 monolayers, which remains approximately constant during their lateral spreading. The observed characteristics of the epitaxial growth are in agreement with a Volmer–Weber mechanism. The Volmer–Weber model was proposed for substrate–overgrowth pairs showing both low adhesion and large linear misfit and, according to it, the formation of 3D-islands requires that the system is highly supersaturated with respect to the overgrowing phase (see [28] and references therein). The weak adhesion between substrate and overgrowth would lead to the development of a semi-coherent rather than a coherent interface. The relaxation of the surface of the rhodochrosite 3D-islands will introduce local variations in the bond lengths, which will cause local deviations from the ideal topography on an atomic scale. The effect of such a modification of the ideal nanotopography can explain the decrease in the step advancement rate of the monoloayers growing on top of the 3D-islands and, eventually, the total suppression of the lateral growth.

Thickness values similar to those reported here, corresponding to a number of monolayers in the range between 8 and 10, have been reported by different authors for a number of systems in which epitaxial growth has been observed (growth of otavite on calcite, kutnahorite on calcite, strontianite on celestite, witherite on barite, etc.) [8,16,40,41]. Therefore, the spreading of multilayer 3D-islands on substrates of different composition seems to be energetically favoured in comparison to the lateral advancement of monolayers, even when the match between the lattices is reasonably good. A complete understanding of the causes of the constant and similar thicknesses observed in different systems will require to carry out computer simulations, which are beyond the scope of the present work. This topic will be thoroughly addressed in future works.

The phenomena described can be relevant to the formation of zoning patterns during the growth of solid solutions from multicomponent aqueous solutions. The development of zoning in minerals, and specifically in carbonates, has been often explained as a result of different situations. Among them, the most significant are: (i) the composition of the solid in equilibrium with an aqueous solution may markedly change if the composition of the solution changes slightly. This behaviour holds for those SS–AS systems with a high difference between the solubility of the solid end members, (ii) the non-ideality of the solid solution, (iii) growth occurring under extremely high supersaturation conditions and (iv) the development of a narrow layer in the solution–crystal interface where rapid changes in composition gradients may occur. This can cause a deviation in the value of the chemical distribution coefficient from the equilibrium value [42,43]. The results of our work suggest that the strain generated as a consequence of lattice mismatch between the substrate and the 3D-islands growing on it exert an important control over the subsequent development of the growth process. In the particular case under consideration, the interface between the calcite substrate and the rhodochrosite thin layer can be regarded as the boundary between two compositional zones in a growing crystal. Once the growth of the

rhodochrosite film ceases as a consequence of the accumulated lattice stress, the physicochemical conditions in the system can become modified. For example, the supersaturation of the aqueous solution may increase leading to the reactivation of growth. The composition of new layers spreading on the surface of the rhodochrosite film may correspond to any member of the calcite–rhodochrosite solid solution, defining another compositional boundary. In the last analysis, a sequence of similar events will lead to the development of oscillatory compositional patterns. Therefore, detailed molecular scale observations of the growth of a precipitate on a substrate of different composition demonstrate that drawing a general picture of the formation of zoned crystals, the structural and compositional characteristics of surfaces, together with the composition and the saturation state of the aqueous solution need to be taken into consideration.

5. Conclusions

In situ atomic force microscope observations have shown that when a calcite $(10\bar{1}4)$ surface is in contact with aqueous solutions highly supersaturated with respect to rhodochrosite ($\beta_{rhod} > 100$), a two-dimensional nucleation rapidly occurs, immediately followed by the dissolution of these nuclei and the formation of three-dimensional islands. If $\beta_{rhod} < 100$ supersaturation, the initial event of two-dimensional nucleation is not observed. The two-dimensional nuclei are interpreted as Mn-hydroxide, while the nature of three-dimensional islands corresponds to rhodochrosite.

Although in all the experiments carried out the Mn-bearing aqueous solution was undersaturated with respect to calcite, dissolution was never observed on the calcite $(10\bar{1}4)$ surface. This is interpreted as a consequence of the blocking of specific sites on calcite surface due to a very effective adsorption of Mn^{2+} and CO_3^{2-} on them.

The islands of the newly formed rhodochrosite show an evident epitaxial relationship with the calcite substrate, growing elongated along $[42\bar{1}]$, although this is the direction of greatest lattice mismatch. Such an apparently anomalous elongation is likely related to the elastic properties of the overgrowth and to the degree of coherence of its interface with the substrate.

The rhodochrosite islands become three-dimensional from the very beginning of their formation, showing a constant thickness equivalent to around 8 monolayers. The characteristics of the epitaxial growth are in agreement with those of the Volmer–Weber mechanism. Although the causes of the constant thickness of islands are difficult to explain, the most probable answer is that an eight-layer configuration is energetically advantageous. An in-depth explanation of the factors underlying the tendency observed in different systems of the formation of epitaxial three-dimensional islands that maintain a constant height during their growth will be required carrying out computer simulations.

The growth and coalescence of these 3D-islands leads to the complete coating of the calcite substrate by a highly homogeneous nanometric layer. As a result of the uniformity in height of this layer, it reproduces every nanotopographic detail of the substrate, such as the cleavage and etch pit steps. Such reproduction resembles the so-called "template effect", a nanoscale phenomenon observed at great length in mineral–multicomponent aqueous solutions systems [4,6,44].

The generation of lattice mismatch between the growing and the underlying layers can cause a deviation in the chemical distribution coefficient from the equilibrium value and lead to the development of compositional zoning in crystals growing from multicomponent aqueous solutions.

Acknowledgements

I. Sethmann and an anonymous reviewer provided constructive reviews that significantly improved the manuscript. We also wish to acknowledge the contribution of M. Hochella Jr. and G. Jordan in offering valuable suggestions and stimulating discussion during the course of this work. Financial support through the Spanish Ministry of Science and Innovation (Project CGL2007-65523-C02-01) and the Comunidad de Madrid (Project CAM-2006-910148) is gratefully acknowledged. The Spanish Ministry of Science and Innovation has also provided financial supported to Carlos Pérez-Garrido through a FPI grant. We sincerely thank the Centro de Microscopia (UCM) for kindly providing us access to the AFM and for technical assistance.

References

[1] C.J. Allègre, A. Provost, C. Jaupart, Nature 294 (1981) 223.
[2] A. Putnis, M. Prieto, L. Fernández-Díaz, Nature 358 (1992) 743.
[3] T. Holten, B. Jamtveit, P. Meakin, Geochim. Cosmochim. Acta 64 (2000) 1893.
[4] J.M. Astilleros, C.M. Pina, L. Fernández-Díaz, A. Putnis, Surf. Sci. 545 (2003) L767.
[5] S.R. Higgins, X. Hu, Geochim. Cosmochim. Acta 69 (2005) 2085.
[6] J.M. Astilleros, C.M. Pina, L. Fernández-Díaz, A. Putnis, Geochim. Cosmochim. Acta 66 (2002) 3177.
[7] C.M. Pina, L. Fernández-Díaz, M. Prieto, A. Putnis, Geochim. Cosmochim. Acta 64 (2000) 215.
[8] C. Pérez-Garrido, L. Fernández-Díaz, C.M. Pina, M. Prieto, Surf. Sci. 601 (2007) 5499.
[9] N. Sánchez Pastor, C.M. Pina, J.M. Astilleros, L. Fernández-Díaz, A. Putnis, Surf. Sci. 581 (2–3) (2005) 225.
[10] A.G. Shtukenberg, J.M. Astilleros, A. Putnis, Surf. Sci. 590 (2005) 212.
[11] E.N. Maslen, V.A. Streltsov, N.R. Streltsova, N. Ishizawa, Acta Crystallogr B 51 (1995) 929.
[12] M.E. Böttcher, Solids State Ionics 101–103 (1997) 1263.
[13] M.K. McBeath, P.A. Rock, W.H. Casey, G.K. Mandell, Geochim. Cosmochim. Acta 62 (1998) 2799.
[14] D.L. Jensen, J.K. Boddum, J.C. Tjell, T.H. Christensen, Appl. Geochem. 17 (2002) 503.
[15] Y.-S. Jun, T.A. Kendall, T.M. Scot, C.M. Friend, J.J. Vlassak, Environ. Sci. Technol. 39 (2005) 1239.
[16] A.S. Lea, T.T. Hurt, A. El-Azab, J.E. Amonette, D.R. Baer, Surf. Sci. 524 (2003) 63.
[17] D.L. Parkhurst, C.A.J. Appelo, User's Guide to PHREEQC, US Geological Survey Water Resources, Investigations Report 99-4259, US Geological Survey, Washington DC, 1999.
[18] P.E. Hillner, A.J. Gratz, S. Manne, P.K. Hansma, Geology 20 (1992) 359.
[19] S.L. Stipp, C.M. Eggleston, B.S. Nielsen, Geochim. Cosmochim. Acta 58 (1994) 3023.
[20] Y. Liang, A.S. Lea, D.R. Baer, M.H. Engelhard, Surf. Sci. 351 (1996) 172.
[21] G. Jordan, W. Rammensee, Geochim. Cosmochim. Acta 62 (1998) 941.
[22] W.M.M. Heijnen, N. Jb. Miner. Mh. 8 (1985) 357.
[23] J. Paquette, R.J. Reeder, Geology 18 (1990) 1244.
[24] W.J. Staudt, R.J. Reeder, M.A.A. Schoonen, Geochim. Cosmochim. Acta 58 (1994) 2087.
[25] R.J. Reeder, J. Rakovan, Surface structural controls on trace element incorporation during crystal growth, in: B. Jamtveit, P. Meakin (Eds.), Growth, Dissolution and Pattern Formation in Geosystems, Kluwer Academic Publishers, 1999, p. 143.
[26] G. Jordan, S.R. Higgins, C.M. Eggleston, K.G. Knauss, W. Schmahl, Geochim. Cosmochim. Acta 65 (2001) 4257.
[27] N.H. DeLeeuw, S.C. Parker, Phys. Rev. B 60 (1999) 13792.
[28] A.A. Chernov, Modern Crystallography III: Crystal Growth, Springer Series in Solid-State Sciences, vol. 36, Springer-Verlag, Berlin, 1984 (Chapter 4).
[29] S.G. Terjesen, J. Erga, G. Thorsen, A. Ve, Chem. Eng. Sci. 14 (1961) 277.
[30] A. Gutjahr, H. Dabringhaus, R. Lacmann, J. Crystal Growth 158 (1996) 310.
[31] A.S. Lea, J.E. Amonette, D.R. Baer, Y. Liang, N.G. Colton, Geochim. Cosmochim. Acta 65 (2001) 369.
[32] M.D. Vinson, R.S. Arvidson, A. Luttge, J. Crystal Growth 307 (2007) 116.
[33] M.B. Hay, R.K. Workman, S. Manne, Langmuir 19 (2003) 3727.
[34] J. Paquette, R.J. Reeder, Geochim. Cosmochim. Acta 59 (1995) 735.
[35] I. Sunagawa, Morphology of minerals, in: I. Sunagawa (Ed.), Morphology of Crystals, Terra Scientific Publishing Company (TERRAPUB), Tokyo, 1987.
[36] C.-C. Chen, C.-C. Lin, L.-G. Liu, S.V. Sinogeikin, J.D. Bass, Am. Mineral. 86 (2001) 1525.
[37] K.J. Davis, P.M. Dove, L.E. Wasylenki, J.J. de Yoreo, Am. Mineral. 89 (2004) 714.
[38] L.E. Wasylenki, P.M. Dove, D.S. Wilson, J.J. De Yoreo, Geochim. Cosmochim. Acta 69 (2005) 3017.
[39] R.S. Arvidson, M. Collier, K.J. Davis, M.D. Vinson, J.E. Amonette, A. Luttge, Geochim. Cosmochim. Acta 70 (2006) 583.

[40] N. Sánchez Pastor, Cristalización secuencial de sulfatos y carbonatos de bario y estroncio a partir de soluciones acuosas: relaciones entre morfología cristalina, composición química y fenómenos de superficie a escala molecular. Ph. D. Thesis. Universidad Complutense de Madrid (2007).
[41] N. Sánchez Pastor, C.M. Pina, L. Fernández-Díaz, Surf. Sci. 601 (2007) 2973.
[42] A.A. Shtenberg, Sov. Phys. Crystallogr. 7 (1) (1962) 92.
[43] P. Ortoleva, Am. Mineral. 94 (2009) 172.
[44] J.M. Astilleros, Estudio integrado de la cristalización de soluciones sólidas no ideales: $(Ca,M)CO_3$ (M=Ba, Sr, Mn). Ph.D. Thesis. Universidad Complutense de Madrid (2001).